Energy Engineering
DOI: xxxxx
Type: XXXX

Unsteady Natural Convection Within an Attic-Shaped Space Subject to Sinusoidal Heat Flux on Inclined Walls

Suvash C. Saha[1,*], Ali M. Sefidan[2] and Atta Sojoudi[3]

[1]School of Mechanical and Mechatronic Engineering, University of Technology Sydney, Ultimo, NSW, Australia
[2]Mechanical Engineering Department, University of Canterbury, Christchurch, New Zealand
[3]Mechanical engineering department, University of Tehran, Tehran, Iran
[*]Corresponding Author: Suvash C. Saha. Email: Suvash.Saha@uts.edu.au
Received: XXXX; Accepted: XXXX.

Abstract: Free convection inside an attic enclosure in which sinusoidal heat flux applied on the inclined walls and a constant temperature applied on the base wall has been investigated numerically to demonstrate the primary flow characteristics and heat transfer within the attic enclosure over daily routine cycles. To solve the governing equations, the finite volume technique has been utilized. After performing the grid independency and time step size tests, the roles of Rayleigh number (Ra) and the attic aspect ratio (AR) on the unsteady flow structure and heat transfer phenomenon are explained for a constant Prandtl number (0.72) for the air. Results are illustrated as a form of stream function and isotherms. Moreover, heat transfer is calculated in terms of Nusselt number. The numerical simulations reveal stratified flow within the enclosure during the daytime nonlinear heating stage. However, during night-time, nonlinear cooling stage the flow turns into unstable as the forms of rising and sinking plumes for sufficiently higher Rayleigh number.

Keywords: Natural Convection; Sinusoidal Heat Flux Condition; Attic-Shaped Spaces.

1 Introduction

During past two decades, research related to the free convection inside enclosures has been received extensive attention because of its significance and importance in industry and in nature. Different enclosures like rectangular, annular or cylindrical spaces etc., exposed to various thermal conditions have been researched utilizing profitable working fluids like air and water. An extensive analysis and review of the above studies can be found in [1-4]. Absolutely, the models related to the rectangular spaces cannot foresee the full buoyancy driven flow inside configurations with irregular or inclined boundaries. Despite the fact that, free convection inside the rectangular type of enclosure has been enormously investigated during the recent years. However, less attention has been given to investigate natural convection in an enclosure like attic shaped under different thermal and flow conditions.

According to climate conditions in different parts of the world, roof of the attic shaped houses receive various thermal effects at different times of the day or different seasons of the year (e.g. winter and summer). Therefore, flow pattern and heat transfer, which are generally governed by the natural convection process should be well understood to make the house comfort for whole day or whole year. It is evident that natural convection is affected by combination of factors such as boundary conditions, the interior structure, geometry shape or size and so on. Heat transfer inside the attic enclosure plays an important role for the thermal effect to the occupants of the buildings. Moreover, a day-to-day change in weather condition leads to various thermal loads in the building structures. Also, the space air conditioning designers have to keep

in their mind that energy consumption should widely be regarded to reduce the amount of waste of energy in buildings.

Isosceles triangular enclosure filled with air was conducted experimentally by Flack [5, 6] by considering different Ra and AR. The enclosure was exposed to cooling/heating conditions from bottom edge or sloping boundaries. Average and local Nusselt number on heated and cooled walls were calculated to study the heat transfer characters through the walls. It was reported that, while the base wall was heated and sloping walls were cooled the laminar natural convection achieved to a critical Ra and became unstable, in which flow pattern changed to the turbulent natural convection regime by increasing the Rayleigh number. By imposing the identical boundary conditions mentioned in [5, 6], Kent [7] reported a stable flow even for higher Ra when heat transfer inside the space was monopolized by conduction (day-time heating case). However, for the case of heating by bottom wall and cooling by top walls conditions (night-time), the flow turned into unstable by increasing Ra in which convection mechanism was prevailed unlike the day-time heating case. It is noteworthy that, the numerical investigation of the same boundary conditions as Flack [5, 6] was evaluated by Ridouane et al. [8]. The authors reported a good agreement between numerical and experimental analysis. They exposed the cutting off side of the bottom tips as a form of thermal insulation boundary condition in their studies [9] and found it as higher energy efficient enclosure which consumed minor energy in order to keep the area at assumed temperature.

Numerous studies focused on the night-time attic problems are available in the literature due to the complex flow structure and heat transfer. Poulikakos and Bijan [10] experimentally studied the night-time boundary condition of the unsteady fluid flow within the triangular attic space for high Ra by assuming symmetric flow along the geometric center line in which free convection flows through a half part of the isosceles attic space [11]. However, they reported that the symmetrical flow within the isosceles triangular space was demolished by rising Rayleigh number. As the Ra exceeds the critical value, the symmetrical flow structure converted to the asymmetrical form. Lei et al. [12] studied the evolution of free convection within a triangular cavity due to rapid cooling of the inclined walls and heating of the bottom wall. Their working fluid was water. In order to visualize the flow of their experimental study, they used shadowgraph technique. They also performed the corresponding 2D numerical simulation in their later study [13].

Several studies related to the stability of the flow pattern are also available in the literature [14-17] for attic space problems. The authors found a flow pattern with a single stable cell, which was generated in the core of the area for different boundary conditions. In addition, they discovered that there were some transitional conditions related to AR and Ra when a cell was separated into some smaller cells.

Holtzmann et al. [18] numerically as well as experimentally investigated the flow pattern for an isosceles triangular enclosure for three various aspect ratios (1, 0.5 and 0.2) for night-time boundary conditions. They performed flow visualization process in order to ratify the existence symmetry-breaking pitchfork bifurcation, which increased with the marginal growth in Ra. This scenario is also seen in [19]. Their numerical reports showed that there was a critical Rayleigh number (1.4×10^5) for which a subcritical pitchfork bifurcation was appeared. As a whole, attic shaped problems with the night-time boundary conditions have been studied more in comparison with the day-time thermal condition [6, 20].

Saha et al. [21-25] employed scaling analysis with numerical verifications to investigate the heat transfer and fluid flow inside attic space for sudden and ramp heating/cooling conditions. They described various stages of thermal conditions of the transient flow development within the cavity. Although natural convection flow in a real attic shaped spaces under different weather climates and conditions were experimentally and numerically evaluated, periodic thermal forcing during diurnal cycle has not paid enough attention. Therefore, authors studied the heat transfer and flow structure due to diurnal thermal condition imposed on the inclined walls.

In the present study, free convection inside an attic enclosure under more realistic thermal boundary conditions, diurnal heat flux condition on the inclined walls with a fixed temperature applied on the bottom wall, has been studied utilizing finite volume numerical technique. Effect of Ra and AR on the unsteady

flow and heat transfer structures are presented performing the grid independency and time step size selection tests.

2 Problem Statement

Physical model of this case is displayed in Fig. 1. Half-length of the bottom wall and the height of the cavity were considered as W and H, respectively. Constant temperature of T_0=295K was applied on the bottom edge. Sloping walls were under three different sinusoidal heat flux conditions where P is the period of thermal forcing. For half of the P (day time), left wall receives the sunny heat flux during the day time which had higher amplitude rather than the right wall which was receiving the shadow heat flux. For the remaining time, both slopping walls received same heat flux during the night time. All walls were assumed to be non-slip. Modified Rayleigh number based on heat flux and cavity height was defined as $Ra \approx g\beta q'' H^4/\alpha k\upsilon$. Five different Rayleigh numbers of 10^9, 10^8, 10^7, 10^6 and 10^5, which were less than the critical modified Ra for cavities with three different aspect ratios of 0.2, 0.5 and 1 with a fixed Prandtl number (0.72) were assumed for this study. Five different points, A to E, were located within the cavity to capture the temperature time series. Two tips in the bottom surface were cut off by 5% in length to exclude the singularity effects at these tips in the numerical solution, and at the cutting edges (Fig. 1) non-slip, rigid and adiabatic vertical walls were assumed. We expected that this modification in the geometry will not lead to any noticeable changes on the general flow progress.

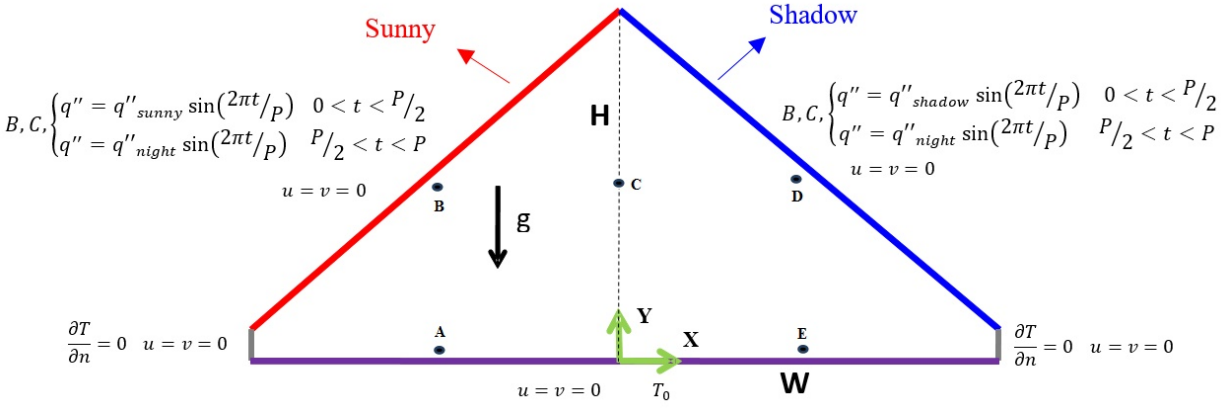

Fig. 1. Physical model

3 Governing Equations and Solution Methodology

The natural air convection through the triangular cavity was calculated from the following set of governing equations including continuity, momentum and energy equations, for which the Boussinesq approximation has been made:

$$\frac{\partial u}{\partial x} + \frac{\partial v}{\partial y} = 0 \tag{1}$$

$$\frac{\partial u}{\partial t} + u\frac{\partial u}{\partial x} + v\frac{\partial u}{\partial y} = -\frac{1}{\rho}\frac{\partial p}{\partial x} + \upsilon\left(\frac{\partial^2 u}{\partial x^2} + \frac{\partial^2 u}{\partial y^2}\right) \tag{2}$$

$$\frac{\partial v}{\partial t} + u\frac{\partial v}{\partial x} + v\frac{\partial v}{\partial y} = -\frac{1}{\rho}\frac{\partial p}{\partial y} + \upsilon\left(\frac{\partial^2 v}{\partial x^2} + \frac{\partial^2 v}{\partial y^2}\right) + g\beta\left(T - T_{ref}\right) \tag{3}$$

$$\frac{\partial T}{\partial t} + u\frac{\partial T}{\partial x} + v\frac{\partial T}{\partial y} = \alpha\left(\frac{\partial^2 u}{\partial x^2} + \frac{\partial^2 u}{\partial y^2}\right) \tag{4}$$

Time step size = 0.5 sec

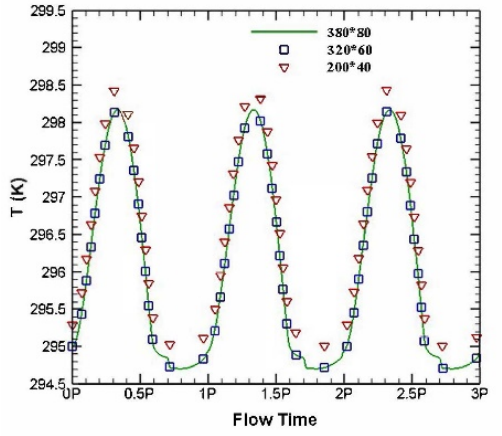

Mesh size = 380×80

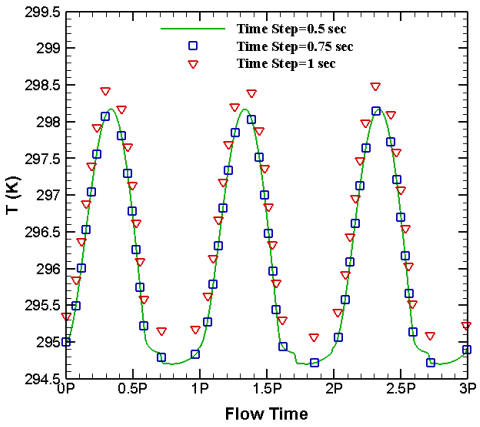

Temperature of point C for AR=0.2, Ra=10^8

Time step size = 0.5 sec

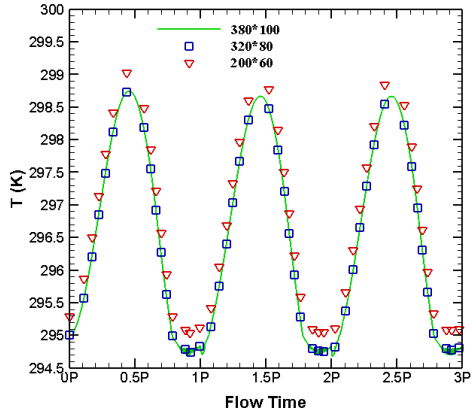

Mesh size = 380×100

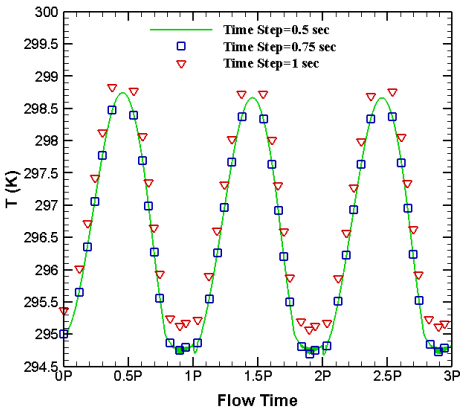

Temperature of point C for AR=0.5, Ra=10^8

Time step size = 0.5 sec

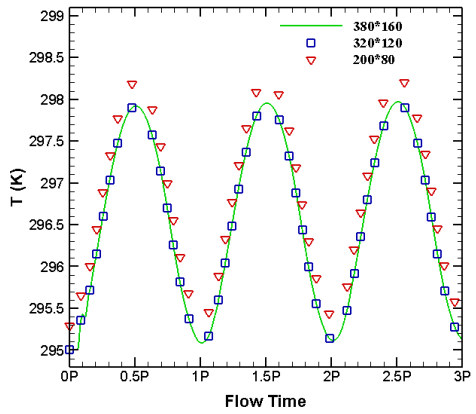

Mesh size = 380×160

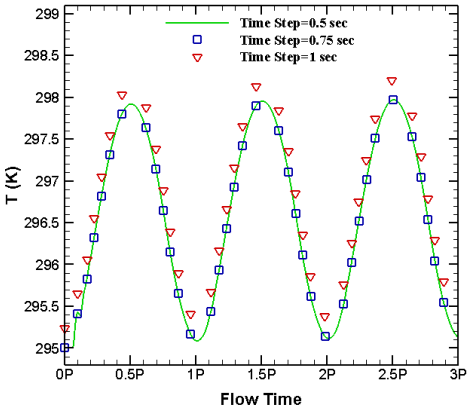

Temperature of point C for AR=1.0, Ra=10^8

Fig. 2. Time step and grid sensitivity test results.

where u and v are the velocity components in x and y directions respectively, t is the time β, α, ρ and ν are coefficient of thermal expansion, thermal diffusivity, density of the fluid and kinematic viscosity respectively, g is the acceleration of the gravity and T is the temperature of fluid.

Eqs. (1) – (4) were solved along with the relevant initial and boundary conditions of this work employing the SIMPLE scheme in ANSYS (Fluent) 17.0. In order to approximation the advection term, the finite volume numerical technique has been selected to discretize the governing equations by the QUICK scheme and central-differencing with second order accuracy were also used to discretize the diffusion terms.

The average Nusselt number for the sloping walls was defined as below:

$$Nu = \frac{h_{eff} L}{k_{air}} \tag{5}$$

where:

$$h_{eff} = \frac{q''}{(T_{\max} - T_{\min})} \tag{6}$$

In which maximum temperature, T_{max}, is sunny wall's locally average temperature at t =2.25P and minimum temperature, T_{min}, is shadow wall's locally average temperature at t =2.75P.

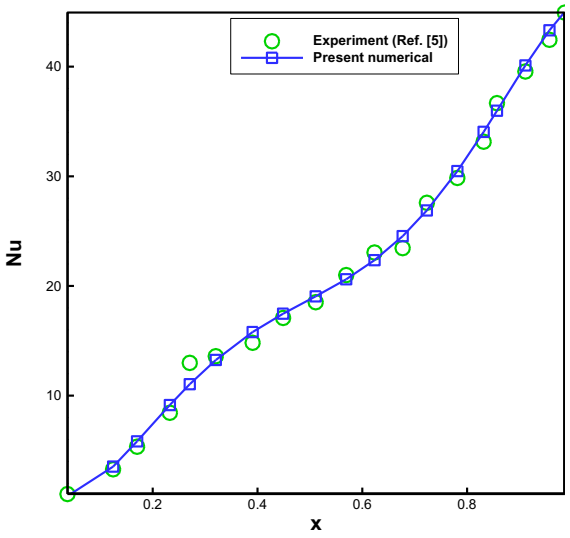

Fig. 3. Distribution of the local Nu along cold wall boundary condition, comparison with experiment [5] (Validation).

4 Time Step and Grid Sensitivity Tests

To check out the appropriate size of grids and a proper time step size, several numerical tests have been conducted. All three AR have been chosen for this evaluation. The results for mesh and time step dependence is shown in Fig. 2. Point *C* was selected within the cavity (See Fig. 1) to measure its temperature and compare it for various mesh sizes and time steps at the fixed Rayleigh number for the full three periods. According to this numerical tests, mesh size of 380×80, 380×100 and 380×160 were selected as a finer mesh for AR=0.2, 0.5 and 1.0 respectively and the time step size of 0.5s has been selected for all three aspect ratios. As Fig. 2. shows, selected grid and time step sizes were small enough to rely on its results. For validate our numerical results, we have also considered a triangular cavity in which bottom wall was adiabatic and inclined walls were maintained in cold and hot constant temperature with Ra=1.5×10^7 and Pr=0.72. We compared the numerical results of local Nu for cold inclined wall with Flack [5] and depicted in Fig. 3. Note that Flack [5] investigated an air-filled cavity including an insulated bottom wall and two hot and cold side walls. For the inclined walls they used constant temperature water tanks in which water

was circulated by pump while one of the inclined walls was heated by heating coils and the other one was kept at the room temperature. It is evident that the numerical results satisfied with the experimental outcomes.

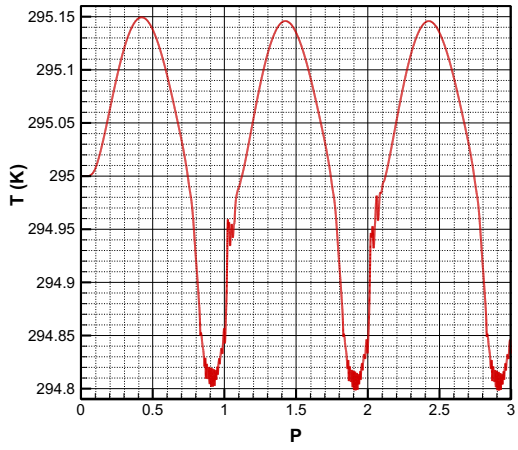

(a) Point A

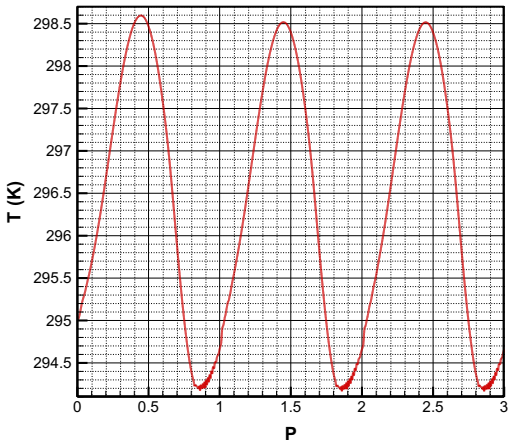

(b) Point B

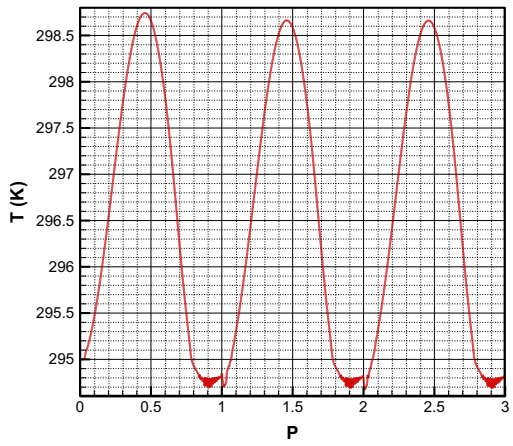

(c) Point C

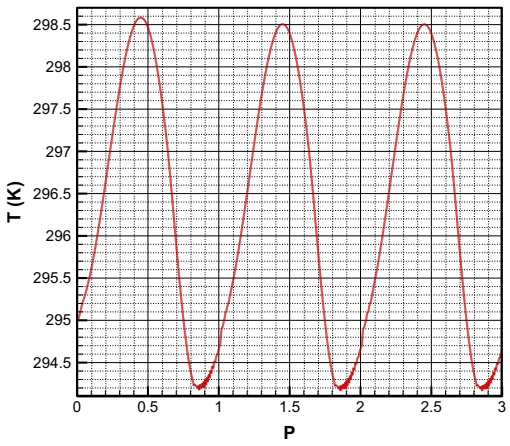

(d) Point D

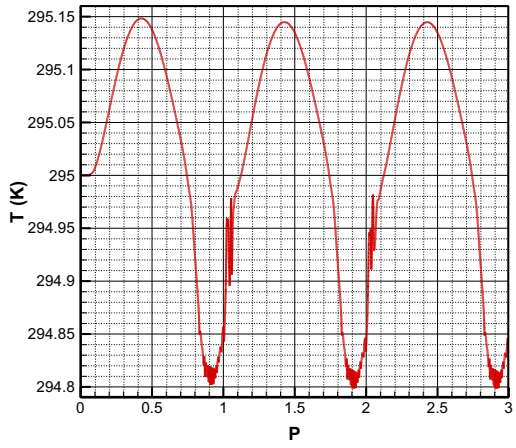

(e) Point E

Fig. 4. Temperature of Points at *AR*=0.5, *Ra*=10^8 a)Point A b)Point B c)Point C d)Point D e)Point E

5 Results and Discussions

Since the initial flow was considered to be stationery and isothermal with the temperature of 295K, starting development of the flow response was definite and we had to lessen these start-up effects. Three complete thermal cycles were measured in this numerical study and it was detected that the starting influence were almost inconsequential and the flow reaction in the 3rd period was similar to that of previous period. Therefore, the results of the last period (3rd period) are illustrated in the next analysis.

5.1 Transient Flow Development

From the asymmetric conditions on inclined walls, we have captured the time developments of the temperature for five different points *A* to *E* in the whole area which are illustrated in Fig. 4 for AR=0.5 and Ra= 10^8. As it is seen from Fig. 1, these points were located at: *A*(-0.5, 0.01), *B*(-0.4955, 0.2410), *C*(0, 0.25), *D*(0.4955, 0.2410) and *E*(-0.5, 0.01). All these points were placed with 1cm spacing from each wall. For the point *A*, which is located near the bottom wall, it is obviously seen that the thermal reaction for the periodic thermal loads on sloping walls is 0.1*P* later for the whole cycles. We can consider this phenomenon as a result of thermo-physical characteristics of the air and the average space between point and walls. In addition, there was a temperature perturbation at the night-time. Because of standing in the other side of the bottom wall, point *E* has almost the same behavior as *A*, both 0.1*P* retarded response and also identical temperature perturbation was seen especially at the night-time. Moreover, the amplitude of the temperature variation in these points is not remarkable, because these two points were placed at the proximity of the bottom wall which was kept at a constant temperature (T_0=295*K*). Point *B* and *D* were close to the sloping walls and there was no lag time found for thermal reaction. Furthermore, not only the amplitude of temperature variation during the whole day greater in comparison with the other points, but also the variation of the day-time temperature was higher than that of the night-time. It can be stated that the point *C* has the combination behaviors of the aforementioned points. There was a temperature disturbance, which was less than those at points *A* and *E* and more than *B* and *D*, and almost 0.4*P* later response for thermal forcing. The other noticeable phenomena about the point C was that, the temperature variation at day-time is almost the same as those at points *B* and *D* but at the night-time due to the remoteness from the inclined walls, temperature variation in this point was not affected.

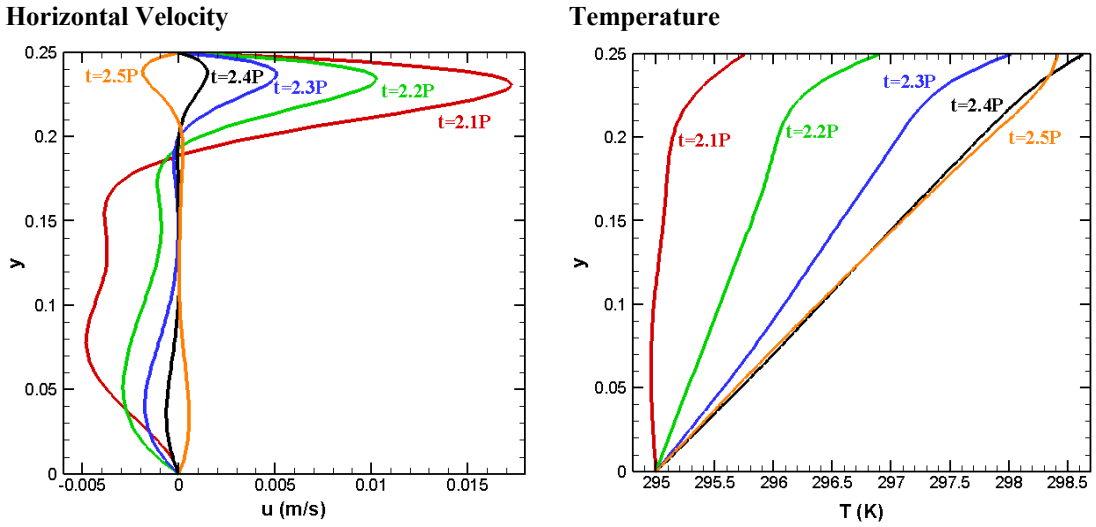

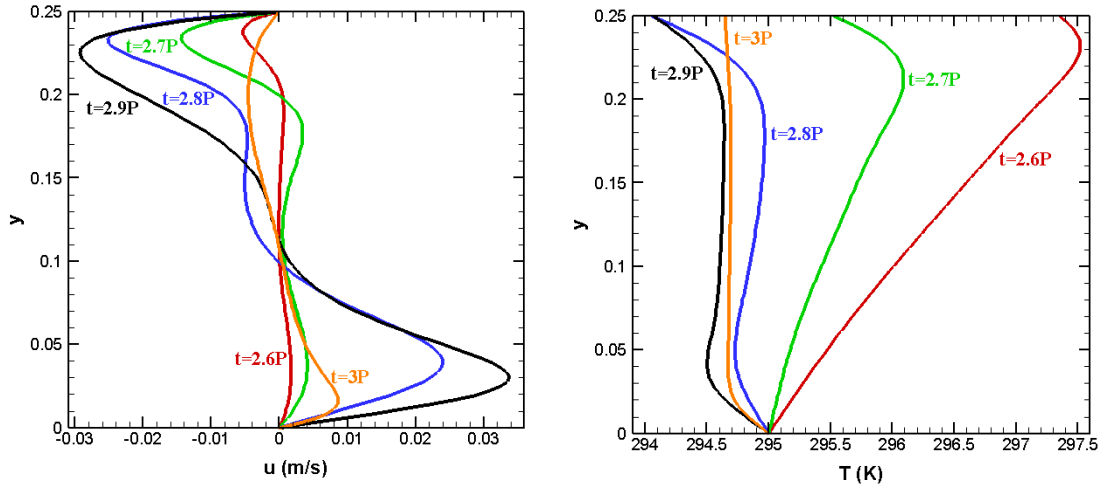

Fig. 5. Horizontal Velocity profile (left) and Temperature profile (right) along AB (The vertical line passing from points A and B) for *AR*=0.5, *Ra*=10^8

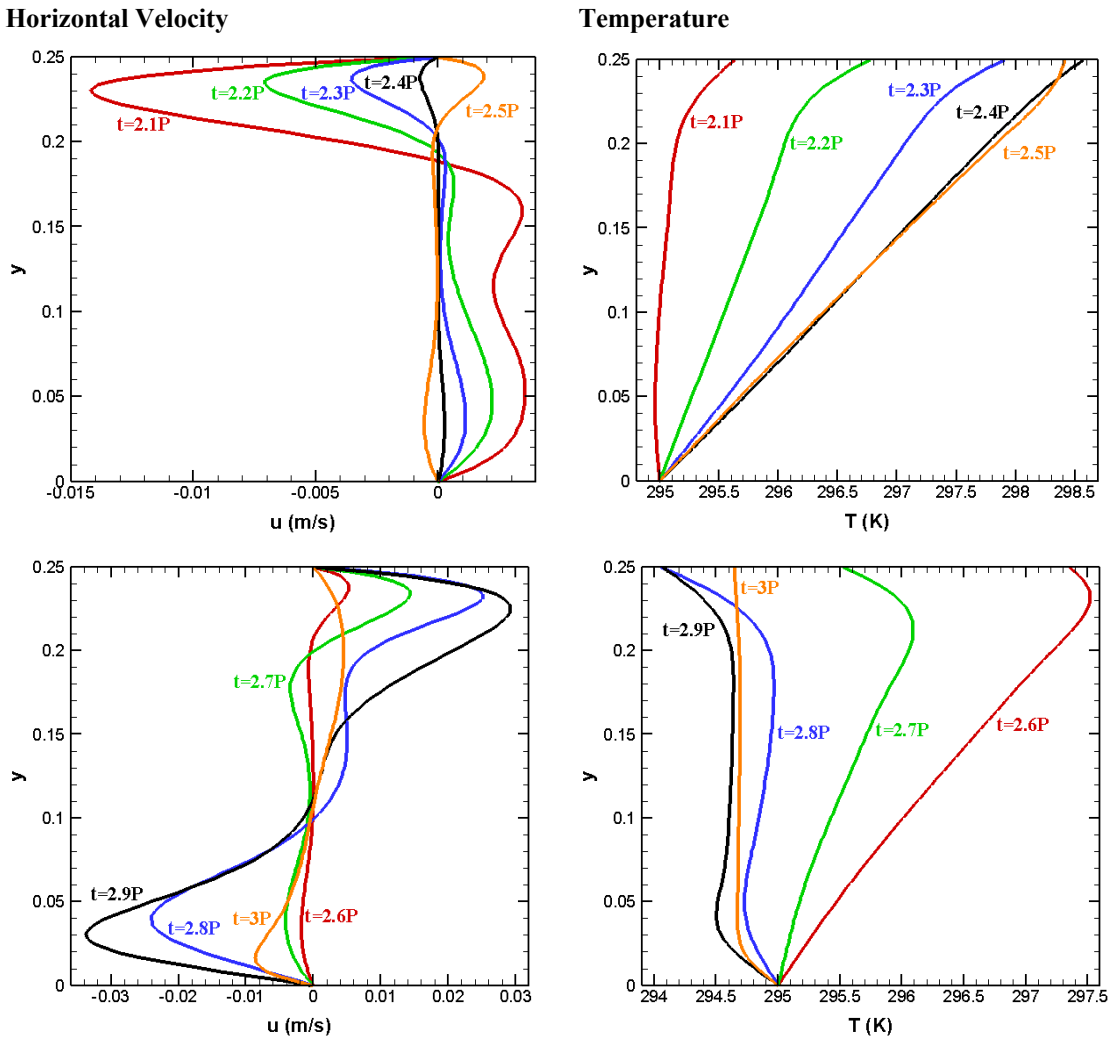

Fig. 6. Horizontal Velocity profile (left) and Temperature profile (right) along DE (The vertical line passing from points D and E) for *AR*=0.5, *Ra*=10^8

Horizontal velocity component and temperature profiles calculated on two different lines which were crossing from the left point *A* and right point *E* and normal to the bottom wall, were displayed in Fig. 5 and 6 over the last period ($2P<t<3P$). Left profiles showed that, a two-layer structure of the horizontal velocity component was formed, and its value became higher near the inclined walls. As seen, these profiles for two different lines were symmetric due to placing in the opposite sides and they behaved in the same way. It was clearly perceived that these layers have oriented to the opposite sides, depicting rotating cells which were spinning in the contrary directions in both corners of the attic. By passing the time, the values of the horizontal velocity components of these layers decreased and approached to zero at the end of the day-time. Then the profile became inverse and the whirling direction of the rotating cells changed to the opposite direction when the night-time started to leave its influences. The rotating velocity of the cells became higher at the new direction, however, it again approached to zero at the end of the night-time reaching to the start-up time of the day condition. During the whole cycle, the highest horizontal velocity was captured at $t=2.9P$ for both top and bottom layers on both lines (with opposing directions). This fact specifies that the rotating velocity of the cells was higher at the night-time rather than that of the day-time at the whole cycle. Temperature profiles for two lines are almost identical and there was an inconsiderable difference between them. It was due to the less difference between thermal forcing on two inclined walls. It was observed that, air temperature increased from the base wall to the sloping wall temperature during the day-time. As the day-time was finished, temperature at the inclined wall was decreased because the nigh-time conditions started to impose on it. This trend had continued up to $t=2.9P$ as the lowest temperature during the whole cycle and then temperature profile was increased to form the start-up condition again at the end of the night-time. It was seen that the highest temperature at the inclined walls occurred at $t=2.4P$ for both lines.

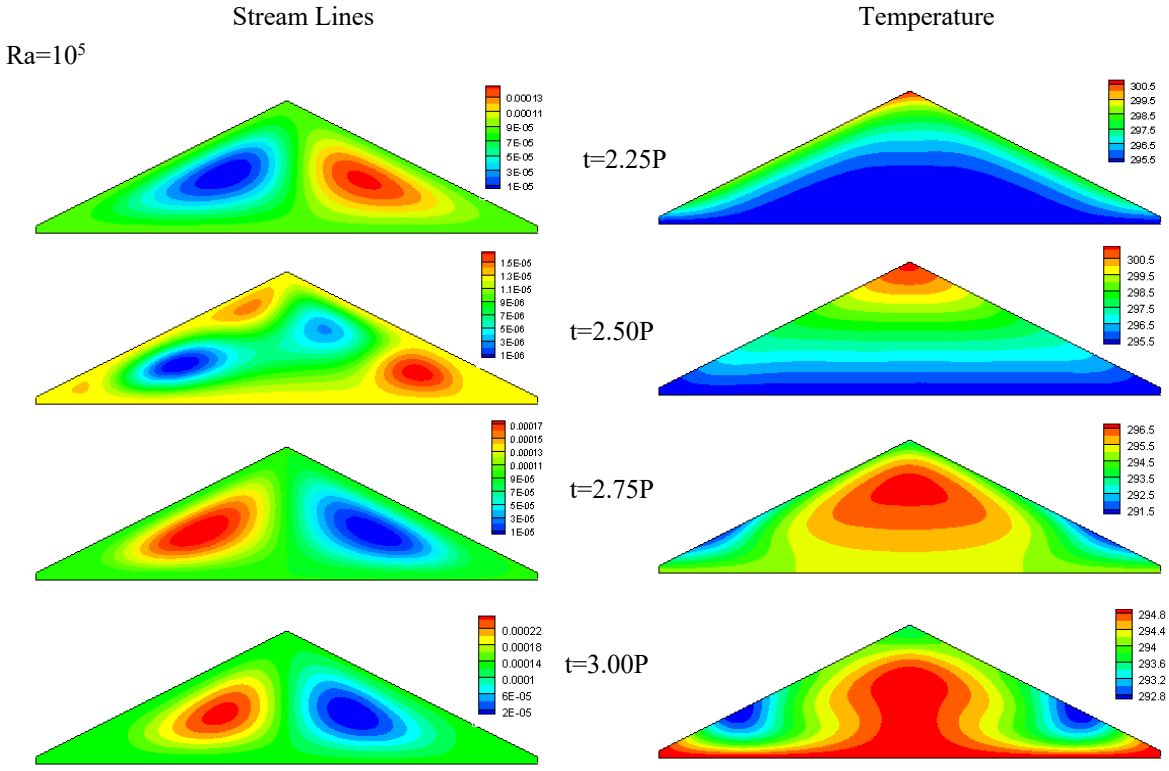

Fig. 7. a

Stream Lines Temperature

Ra=10^6

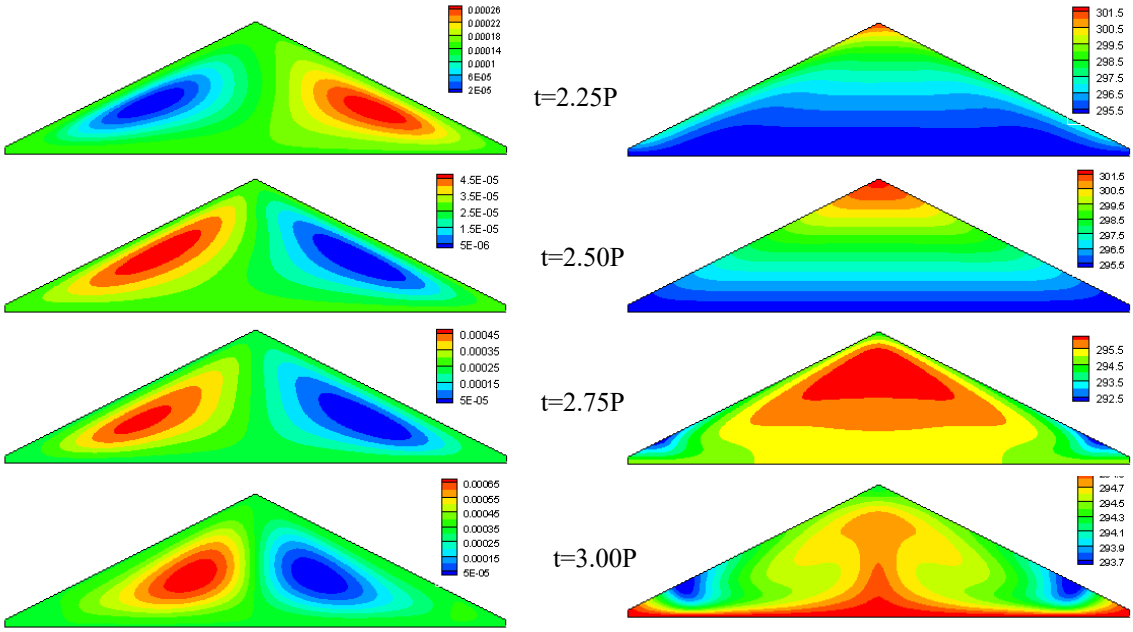

Fig. 7. b

Stream Lines Temperature

Ra=10^7

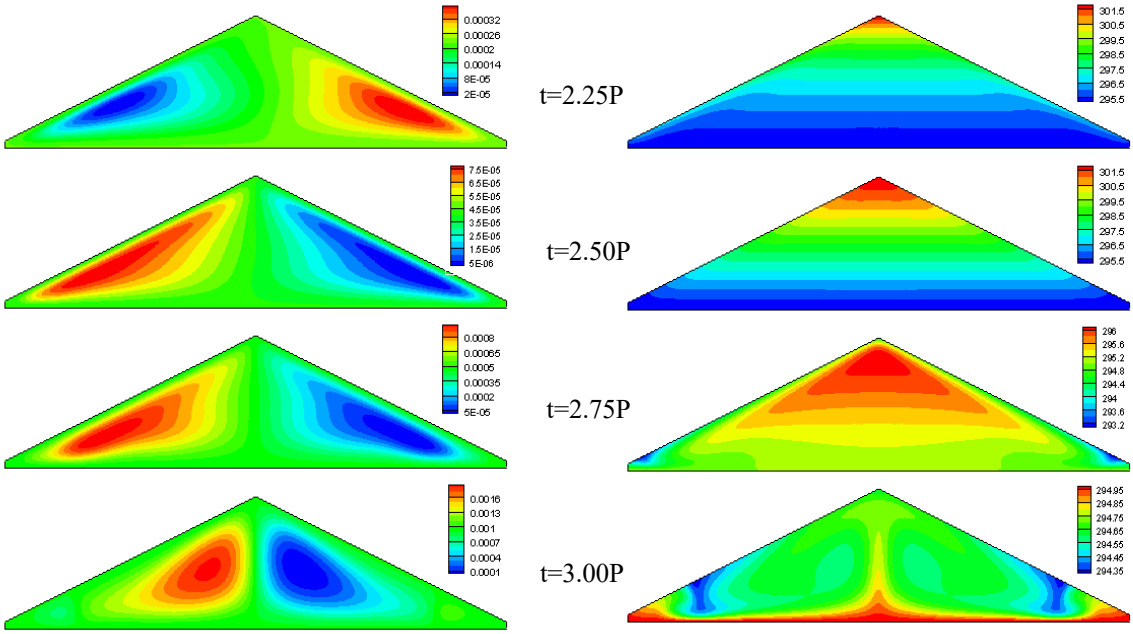

Fig. 7. c

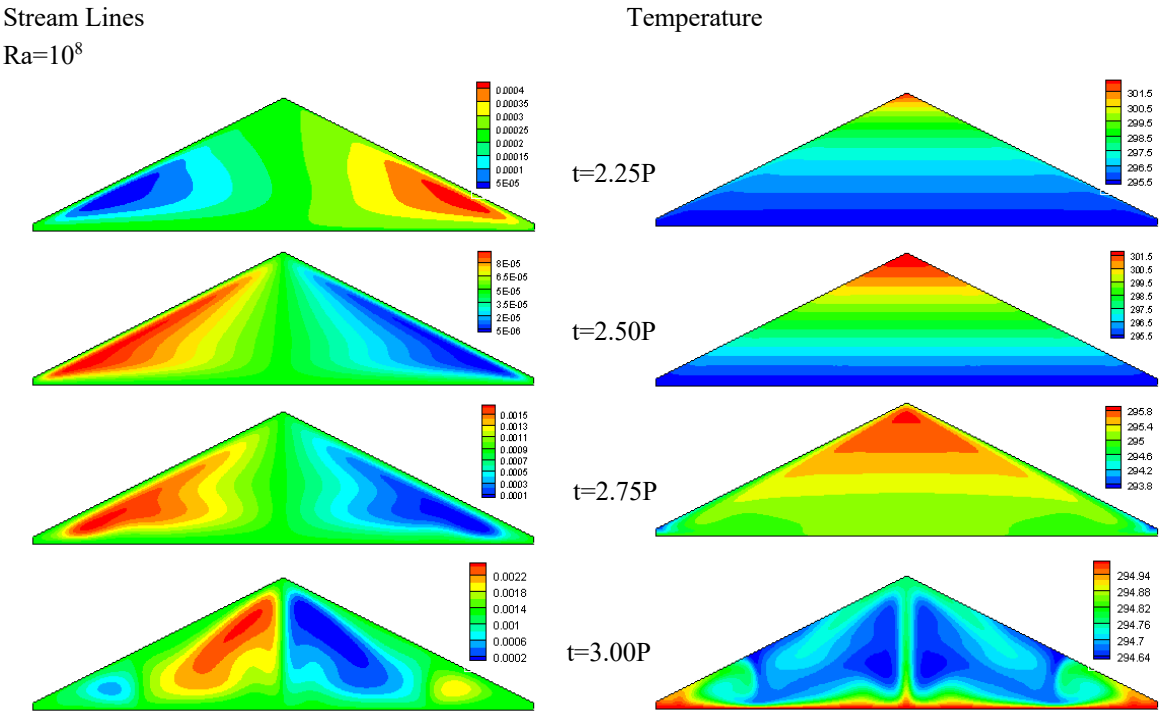

Fig. 7. d

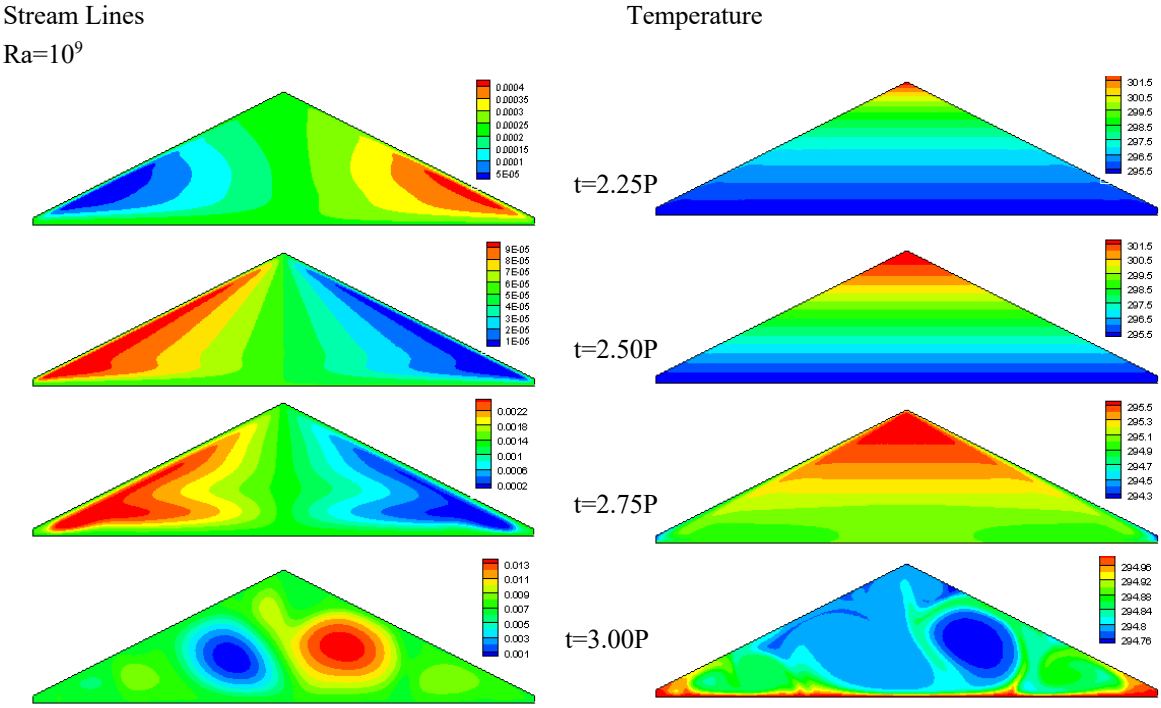

Fig. 7. e

Fig. 7. Snapshots of stream function (Left) and temperature (Right) contours for different times and *AR*=0.5. at a) Ra=10^5 b) Ra=10^6 c) Ra=10^7 d) Ra=10^8 e) Ra=10^9

5.2 Effect of Rayleigh Number

Present study covers a various range of Rayleigh numbers (10^5, 10^6, 10^7 and 10^8). The stream function (left) and the corresponding isothermal contours (right) at t =25P, 2.5P, 2.75P and 3P for fixed AR=0.5 are seen at Fig. 7. These contours show different features of transient flow over these ranges of Rayleigh numbers. As seen from Fig. 7(A), for Ra=10^5 two rotating cells were formed next to the inclined walls for all day and night times which were suffered less deformation over the cycle except at the end of the day which was defaced remarkably. This deformation was originated from the day-time effects which led to pure conduction heat transfer mechanism. Furthermore, this deformation made the average value of stream function decrease too, because while the natural convection was inactivated, cells became weak, and consequently, the value of stream function had fallen. Temperature contours showed the temperature distribution of air during the whole cycle and the reaction of heating and cooling patterns at day and night-time respectively. For the day-time due to heating effects and pure conduction situation, stratified temperature contour was observed. However, by the end of the night-time, when the slopping walls made the air next to them cooler, a plume near the bottom wall was formed. For Ra=10^6, the average value of stream function went up due to stronger natural convection effects. Similarly, this value followed the same upward trend by reaching to larger Ra. Moreover, the value of stream function was low again at the end of the day for higher Ra because of the abovementioned reason. Repeatedly, two rotating cells were formed beside the both inclined walls. Day-time stratified temperature contour was perceived from the day-time effects and rising plume from the bottom wall have been repeated. It is evident that with increasing Ra, natural convection became stronger and consequently, day and night-time effects transmitted to the fluid promptly. As a result, the act of warming up and cooling down of the air has happened fast and the plume had not found sufficient time to be formed.

5.3 Effect of Aspect Ratio

Fig. 8 shows the streamline and temperature contours for different aspect ratios and fixed Ra=10^8 during a whole day cycle. The first key feature which was revealed from this figure was that, for AR=0.2, more cells were formed especially at the night-time from the proximity of the bottom wall and the inclined walls. For day-time when the conduction heat transfer became dominant, stratified temperature contour was reported. As aspect ratio was increased, the numbers of convecting cells were decreased to two cells at the vicinity of each inclined walls.

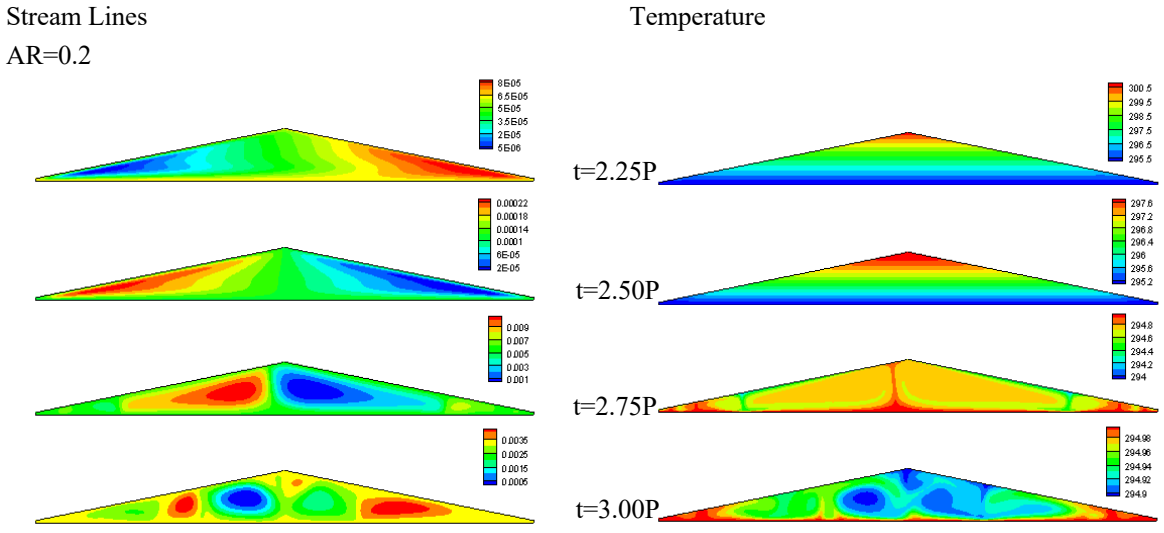

Fig. 8. a

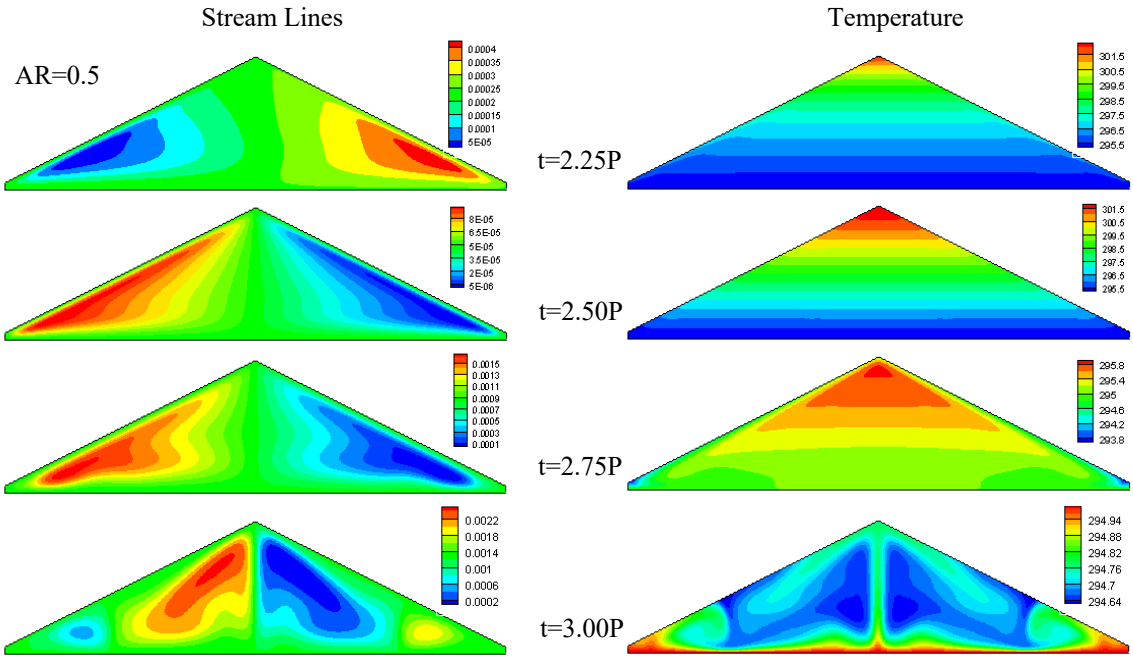

Fig. 8. b

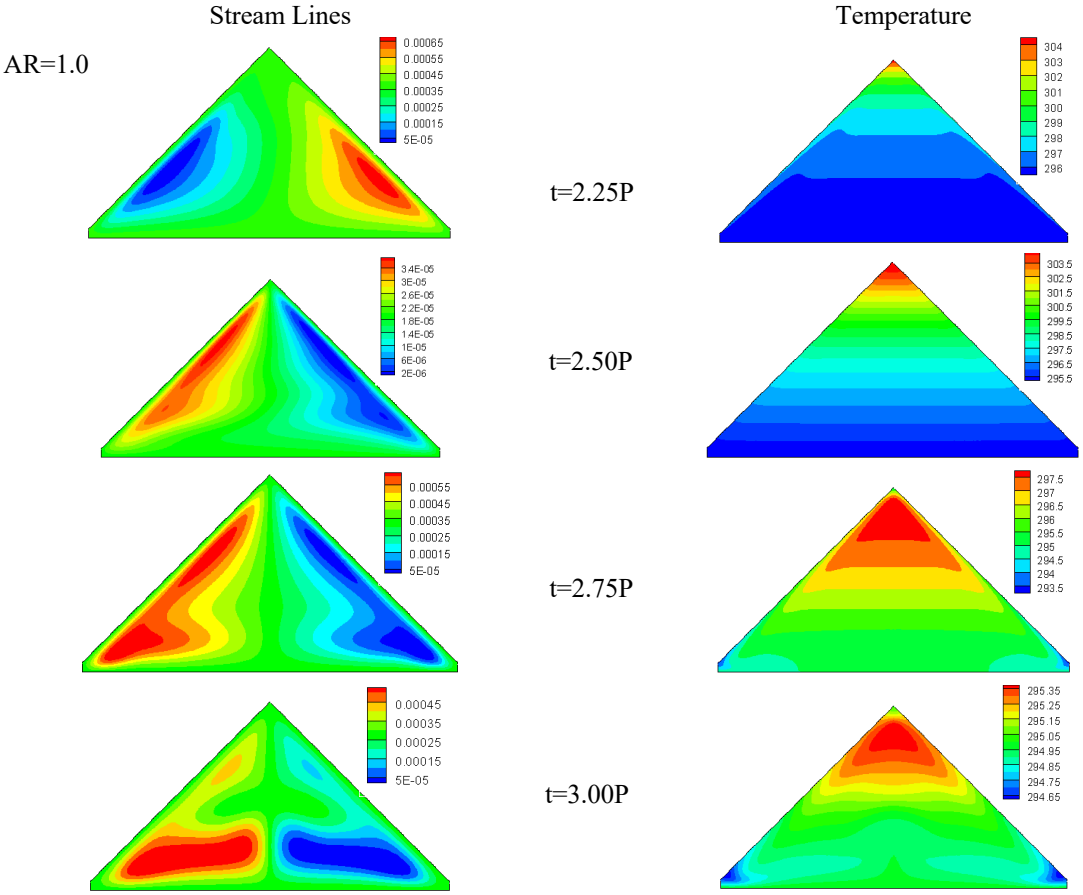

Fig. 8. c

Fig. 8. Snapshots of stream function (Left) and temperature (Right) contours for different times and $Ra=10^8$ at a) AR=0.2 b) AR=0.5 c) AR=1.0

5.4 Heat transfer phenomenon

Fig. 9 represents the average Nusselt number for different Ra and fixed AR=0.5 for shadow, sunny and bottom walls. It is evident that as the Ra increased, the average Nu of all the walls possessed higher amplitude due to the strong thermal forcing. Fig. 9(a) and Fig. 9(b) showed that, the proportion of heat transfer into the cavity at the day-time from sunny wall was higher in comparison with the shadow wall at the same time, however, both of them released the same amount of heat at the night-time. This phenomenon was repeated for the whole Ra.

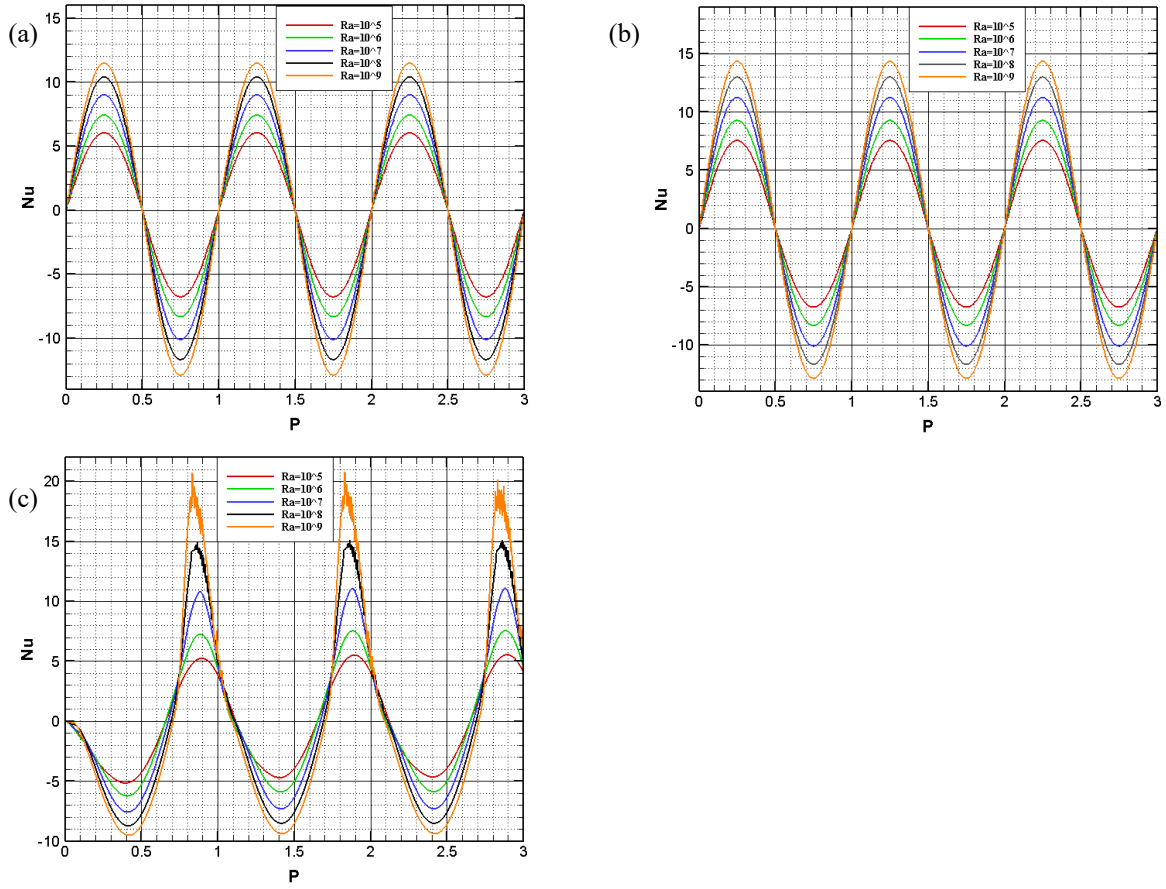

Fig. 9. Average Nusselt number at different *Ra* and *AR*=0.5 for a) Shadow wall b) Sunny wall c) Bottom Wall.

For the bottom wall, the amount of imported and exported heat into and out of the cavity was almost the same for low Ra (Ra= 10^5). Convection heat transfer was the dominant mechanism at the night-time, and conversely, conduction heat transfer was prevailing mechanism at the day-time. As a result, increasing Ra, added some disturbance to convective heat transfer, especially at the higher Ra, but it could not disturb the day-time flow because of inactivated convection mechanism. Therefore, the bottom wall released less heat at the day-time in comparison with gaining it at the night-time. By this way, bottom wall played an effective role in transferring heat into the cavity at the night-time. In this way the energy was conserved. Furthermore, the only boundary which released the heat at the day-time was bottom wall (Fig. 9c).

Fig. 10 displays average Nusselt number at different AR with Ra=10^8 for shadow, sunny and bottom walls. As the aspect ratio increased, the cavity gained heat flux with higher area size, therefore, according to definition of Nu, as it was seen, Nu was increased with the increasing of AR in both sunny and shadow walls. For bottom wall, increasing in AR caused the decreased in Nu. This went back to the proximity of the boundaries in low AR and it can be concluded that, while the achieved heat flux has risen in high AR,

Nu was highly affected by the nearness of the boundaries.

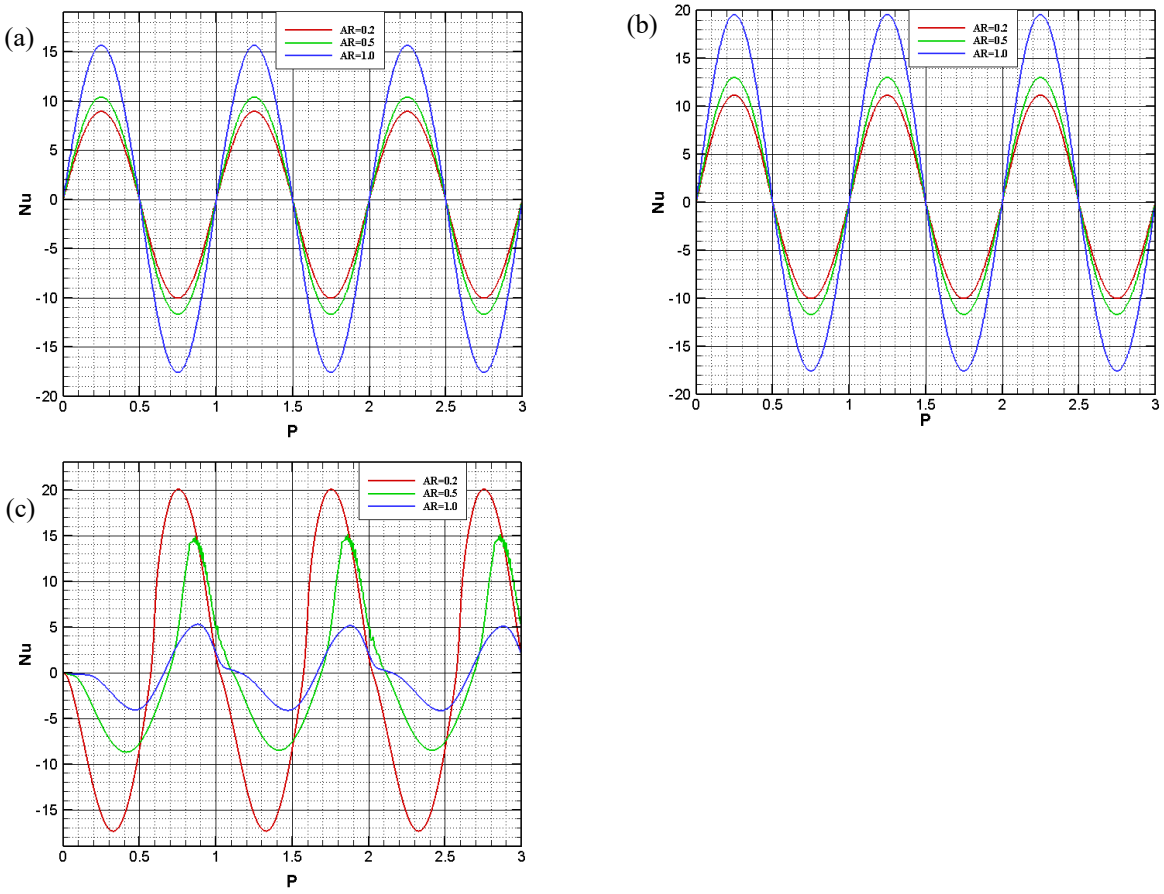

Fig.10. Average Nusselt number at different *AR* and *Ra*=10^8 for a) Shadow wall b) Sunny wall c) Bottom Wall.

6 Conclusions

Natural convection within the attic spaces under daily thermal loads on the inclined walls were investigated numerically using finite volume technique for a various range of Rayleigh numbers ($10^5 \leq$ Ra $\leq 10^9$) and attic aspect ratios ($0.2 \leq$ AR ≤ 1.0). In addition, the effects of Ra and AR on the unsteady flow progress and heat transfer with a fixed Prandtl number of 0.72 for air as the work-fluid was reported. Major outcomes of the present study can be summarized as:

- The numerical results confirm that the temperature contours were stratified for the day-time, however, rising and sinking plumes at the vicinity of bottom wall was captured at night time. This could be attributed to this fact that, the prevailing mechanism at the night-time was convection heat transfer which was inactivated while the day-time conditions imposed.
- As the Ra value increased, the amount of stream function rose in order to strong natural convection effects with the exception of t =2.5P. This went back to the dominant conduction mechanism at the day-time for all Ra.
- With the decreasing of the AR, more cells were formed due to the proximity of the boundaries which led to enhancement of Nu for bottom wall.
- With the increase of Ra, the transferred heat from all boundaries was climbed due to the strong thermal forcing.

- The amount of exported and imported heat transfer from the bottom wall was equal for both night and day-time for lower Ra, but for higher Ra, the amount of heat transfer to the out of the cavity at night-time soared almost as twice as day-time. This can be attributed to this fact that; convection mechanism became disturbed by rising Ra.
- For the fixed Ra, the amount of transferred heat from side walls ascended for higher AR in which cavity could reach higher amount of heat flux.
- The locally average amount of Nu for bottom wall which was kept at the constant temperature dipped for higher AR, due to the nearness of boundaries for lower AR.

Funding Statement: The author(s) received no specific funding for this study.

Conflicts of Interest: The authors declare that they have no conflicts of interest to report regarding the present study.

References

1. Patterson, J. C., Imberger, J., (1980). Unsteady natural convection in a rectangular cavity. *Journal of Fluid Mechanics, 100*, 65-86.
2. Oztop, H. F., Abu-Nada. E., (2008). Numerical study of natural convection in partially heated rectangular enclosures filled with nanofluids. *International Journal of Heat and Fluid Flow* 29.5, 1326-1336.
3. Oztop, H. F., Estellé, P., Yan, W. M., Al-Salem, K., Orfi, J., Mahian, (2015) A brief review of natural convection in enclosures under localized heating with and without nanofluids. *International Communications in Heat and Mass Transfer*, 60, 37-44.
4. Yin, S. H., Wung, T. Y., Chen, K., (1978). Natural convection in an air layer enclosed within rectangular cavities. *International Journal of Heat and Mass Transfer* 21.3, 307-315.
5. Flack, R. D., (1980). The experimental measurement of natural convection heat transfer in triangular enclosures heated or cooled from below, *Trans. ASME: J. Heat Transfer*, 102, 770–772.
6. Flack, R. D., Witt, C. L., (1979). Velocity measurements in two natural convection air flows using a laser velocimeter. *Journal of Heat Transfer*, 101(2), 256-260.
7. Kent, E. F., (2009). Numerical analysis of laminar natural convection in isosceles triangular enclosures. *Proceedings of the Institution of Mechanical Engineers, Part C: Journal of Mechanical Engineering Science*, 223(5), 1157-1169.
8. Ridouane, E. H., Campo, A., McGarry, M., (2005). Numerical computation of buoyant airflows confined to attic spaces under opposing hot and cold wall conditions. *International Journal of Thermal Sciences*, 44(10), 944-952.
9. Ridouane, E. H., Campo, A., Hasnaoui, M., (2006). Benefits derivable from connecting the bottom and top walls of attic enclosures with insulated vertical side walls. *Numerical Heat Transfer, Part A: Applications,* 49(2), 175-193.
10. Poulikakos, D., Bejan, A., (1983). Natural convection experiments in a triangular enclosure. *Journal of heat transfer*, 105(3), 652-655.
11. Poulikakos, D., Bejan, A., (1983). The fluid dynamics of an attic space. *Journal of Fluid Mechanics,* 131, 251-269.
12. Lei, C., Xu, F., Patterson, J. C., (2005). Visualisation of natural convection in an isosceles triangular enclosure heated from below. In: *Proceedings of the 5th Pacific Symposium on Flow Visualisation and Image Processing*, 27 - 29 September 2005, Daydream Island, QLD, Australia.
13. Lei, C., Armfield, S. W., Patterson, J. C., (2008). Unsteady natural convection in a water-filled isosceles triangular enclosure heated from below. *International Journal of Heat and Mass Transfer*, 51(11), 2637-2650.

14. Salmun, H., (1995). The stability of a single-cell steady-state solution in a triangular enclosure. *International journal of heat and mass transfer*, 38(2), 363-369.
15. Farrow, D. E., Patterson, J. C., (1993). On the response of a reservoir sidearm to diurnal heating and cooling. *Journal of Fluid Mechanics*, 246, 143-161.
16. Asan, H., Namli, L., (2001). Numerical simulation of buoyant flow in a roof of triangular cross-section under winter day boundary conditions. *Energy and Buildings*, 33(7), 753-757.
17. Asan, H., Namli, L., (2000). Laminar natural convection in a pitched roof of triangular cross-section: summer day boundary conditions. *Energy and Buildings*, 33(1), 69-73.
18. Holtzman, G. A., Hill, R. W., Ball, K. S., (2000). Laminar natural convection in isosceles triangular enclosures heated from below and symmetrically cooled from above. *Journal of Heat Transfer*, 122(3), 485-491.
19. Ridouane, E. H., Campo, A., (2006). Formation of a pitchfork bifurcation in thermal convection flow inside an isosceles triangular cavity. *Physics of Fluids*, 18(7), 074102.
20. Akinsete, V. A., Coleman, T. A., (1982). Heat transfer by steady laminar free convection in triangular enclosures. *International Journal of Heat and Mass Transfer*, 25(7), 991-998.
21. Saha, S. C. (2011). Unsteady natural convection in a triangular enclosure under isothermal heating. *Energy and Buildings*, 43(2), 695-703.
22. Saha, S. C. (2011). Scaling of free convection heat transfer in a triangular cavity for Pr> 1. *Energy and Buildings*, 43(10), 2908-2917.
23. Saha, S. C., Patterson, J. C., Lei, C., (2010). Natural convection in attics subject to instantaneous and ramp cooling boundary conditions. *Energy and Buildings*, 42(8), 1192-1204.
24. Saha, S. C., Patterson, J. C., Lei, C., (2010). Natural convection in attic-shaped spaces subject to sudden and ramp heating boundary conditions. *Heat and Mass Transfer*, 46(6), 621-638.
25. Saha, S. C., Patterson, J. C., Lei, C., (2010). Natural convection in attics subject to instantaneous and ramp cooling boundary conditions. *Energy and Buildings*, 42(8), 1192-1204.